THE JOURNAL OF NAVIGATION (2011), **64**, 29–44. © The Royal Institute of Navigation
doi:10.1017/S0373463310000378

Waypoint Navigation of Small-Scale UAV incorporating Dynamic Soaring

O. K. Ariff and T. H. Go

(*Nanyang Technological University*, *Singapore*)
(Email: OMAR@ntu.edu.sg)

The latest attempts at improving small scale autonomously guided Uninhabited Aerial Vehicles (UAVs) have concentrated around the increase of range and speed. One of these ways is to incorporate dynamic slope soaring manoeuvres as part of the flight path. This is in contrast to most conventional path-planning algorithms where waypoint guidance is merged with terrain avoidance or contour following capability. Additionally, current trajectory optimization techniques are iterative and so have a considerable computational load. The proposed algorithm is based on Dubin's curves, and is therefore optimal by definition. Being non-iterative, it is comparatively a more efficient algorithm. Hence, a key advantage of the proposed technique is that the desired trajectory is generated quickly in real time with minimum computational load while satisfying the spatial constraints of dynamic slope soaring.

KEY WORDS

1. dynamic soaring. 2. path planning algorithm. 3. Dubin's curve. 4. differential geometry.

1. INTRODUCTION. In proposing this algorithm, we have focused upon recent trends in the development of UAVs. The trend for tactical UAVs has been towards versatility, small size, long range coupled with high speed, and long endurance. During conflict tactical small-scale UAVs, which do not require runways and are operated by small units of ground forces, are just as critical for battle as large, strategically deployed UAVs. Hence, the primary objective of today's research and development is to ensure that small-scale tactical UAVs have the range, speed and endurance of platforms several times larger. Key changes in the area of design, propulsion and navigation algorithms are all targeted towards this aim. Great emphasis has been placed on the ability to extend speed and range for small-scale tactical UAVs i.e. with a wingspan of less than 2·5 m and maximum total take-off weight of 5 kg. Payload carrying capacity is less important as sensors continue to get smaller. UAVs of this class stand to benefit from the development of automatic soaring navigation and control algorithms, since soaring would enable greater range and endurance – performance measures that are important to their most popular role of reconnaissance.

The paper is organized as follows. Section 2 begins by defining the different modes of soaring and explains why dynamic soaring is relevant to small scale tactical UAVs deployed specifically for over-the-hill tactical reconnaissance missions. It also reviews

the work which has been carried out in the fields of study related to the scenario addressed in this paper. These areas are autonomous soaring, trajectory formation and real-time computation. In the second part of the section, it then proceeds to explain how none of the work done to date addresses all the issues and constraints simultaneously. In contrast, it must be emphasized at this juncture that the key contribution here is derivation of a computationally unintensive algorithm which includes dynamic soaring in its waypoint algorithm while utilizing but not concerning itself with the heuristics of the dynamic soaring manoeuvre itself. The final part of section 2 explains why a heuristic model of dynamic soaring is needed, and qualitatively and quantitatively assesses the different heuristic models available of dynamic soaring. Based on this, specific criteria were drawn out to determine the necessary and sufficient conditions to be satisfied by such a model. It then justifies the selection and use of a hybrid heuristics model.

Section 3 begins by introducing key parameters of curvature and torsion within the context of differential geometry. In the second part, it explains how the Dubin's curve derived from principles of differential geometry satisfies the necessary and sufficient conditions for a solution. Section 4 then utilizes these principles to derive an algorithm that generates such a class of trajectories. Section 5 defines two test cases used to demonstrate the outcome of the trajectory generation algorithm by simulation. It also explains the resulting trajectory plots, and discusses the key aspects of the results. Section 6 finally concludes the paper by summarizing the keys points and provides recommendations for future work.

2. DYNAMIC SOARING FLIGHT.

2.1. *Soaring flight*. The primary objective of soaring is to demonstrate improvement in one of the two areas which would in effect improve the performance of a small-scale UAV performing two differing mission types. The first area of improvement is extended range and endurance for surveillance and loiter mission type. The second is extended range due to higher speed for point-to-point reconnaissance mission type. In parallel, there are three types of soaring, thermal, ridge and dynamic, which are used by UAVs utilizing airframes of the powered glider configuration.

The first mission type achieves enhanced performance through additional lift. Hence, thermal and ridge soaring are utilized for such missions. The additional gain is apparent and explicit. With an addition in lift, the required forward speed in order to maintain straight and level flight can be reduced. This would be an advantage in loiter missions. The second mission type achieves enhanced performance through an increase in speed. This can be achieved through dynamic soaring, and is predominantly an advantage in point-to-point reconnaissance missions.

Most glider pilots are familiar with thermal soaring. Allen addresses the issue of thermal soaring rather well (see Allen, 2006 and Allen, 2007). However, the prerequisites of the existence of thermals are as follows. Firstly, thermals exist in relatively flat terrain. Secondly, weather and climatic conditions in a certain planar area should be well recorded and documented for an autonomous navigation algorithm to be able to effectively utilize such data.

Ridge soaring is extremely effective for providing added lift, and is more applicable in areas with significant land formations such as hills, mountains and ridges as stated (Langelaan, 2007). Hence, it is extremely applicable for loiter missions in areas with

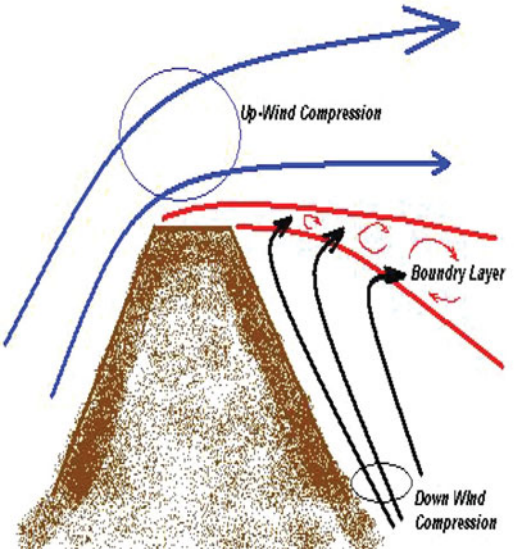

Figure 1. Wind direction on the windward and leeward sides of a geophysical feature.

known terrain profiles but more uncertain and unstable weather conditions. However, ridge soaring does not increase speed and is not relevant for over-the hill tactical missions.

The third type of soaring and the one addressed in this paper is dynamic soaring (see Figure 1). It is defined as flight sustained through the power gained by co-ordinated manoeuvring in wind gradients. More about this method of soaring will be explained in section 2.3. To this effect, it has to be mentioned that gust soaring should also be included in this category as it is energy extraction from gusts. If its heuristics are well known, then it is possible to incorporate it within the stability augmentation/flight control level of the guidance, navigation and control system. Although the gust soaring is effective as proven by Kyle et al (see Kyle, Evans and Costello, 2005), it is also highly unpredictable and difficult to incorporate into a navigation algorithm (see Allen and Lin, 2007). It is however outside the scope of this work.

2.2. *Dynamic soaring algorithm as part of the outer navigation loop.* Dynamic soaring can be over sea or over land. Over land it usually involves performing skewed helical manoeuvres very close to the leeward side of a geophysical formation. Relatively strong wind flowing over the top of the windward side sets up a wind gradient consisting of gradually decreasing wind speed with the downward slope on the leeward side. The trajectory of the manoeuvre is as shown in Figure 2. Radio Controlled (RC) glider pilots have been documented to have manually piloted gliders to achieve extreme acceleration by performing three to ten of these loops. Experimental flight tests by RC enthusiasts have widely demonstrated in the RC world that the unpowered glider of the said configuration can achieve a comfortable speed of more than 360 miles an hour (see Kinetic 100).

We concentrate on dynamic soaring for the following reasons. It is most suitable for use in small scale, tactical UAVs carrying out point-to-point over-the-hill re-connaissance missions. It is robust with respect to weather, and its primary advantage

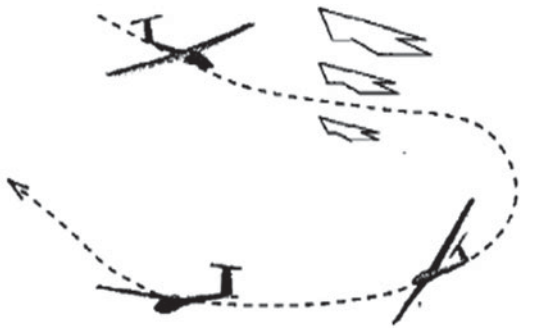

Figure 2. Manoeuvre performed by a dynamic soaring glider (Illustration from Wharrington, 2004).

is the picking up of speed. This is in contrast to ridge and thermal soaring, which is the harnessing of lift. The majority of UAV navigation algorithms implemented today incorporate some form of obstacle avoidance. This means that the trajectory desired in the neighbourhood of the obstacle is to entirely avoid it, albeit within a certain safety distance. To incorporate dynamic soaring, the desired trajectory should essentially be generated where the necessary condition would be to achieve a certain proximity to the land feature or obstacle in question.

To date, much work has been done separately on trajectory optimization, but does not harness Dubin's curves, and not in a dynamic soaring scenario. For example, (Yang and Kapila, 2002) investigated target touring and obstacle avoidance and do not consider dynamic soaring manoeuvres within the trajectory generated. Likewise, (Akram, Pasha and Iqbal, 2005) examine a similar scenario but involving multiple UAVs and including localization uncertainties of INS sensors.

Furthermore, it is critical that any guidance algorithm utilized on such platforms be computationally simple, or else the computational load for such a technique renders it unsuitable for real time implementation on small-scale platforms. Previous work on single UAV path planning as well as multi-UAV formation control and cooperative guidance involve the impractical use of an on-line iterative technique to find the minimum value of a Hamiltonian equation. In (Chitsaz and LaValle, 2007), the temporal constraint was satisfied by applying the Pontryagin principle to a baseline Dubin's curve and solving a resulting Hamiltonian function iteratively. The dynamic soaring scenario considered here does not have a temporal constraint and therefore solving such a function is not required.

Shanmugavel in (Shanmugavel et al 2005, 2009) have derived a rather elegant closed form solution for multiple UAVs in a cooperative guidance scenario where the algorithm satisfies both temporal and spatial constraints. In all the papers the versatility of this form of Dubin's curve has been demonstrated. Hence, it demonstrates that Dubin's curves form a useful basis for the inclusion of dynamic soaring manoeuvres into a trajectory generation algorithm for UAVs.

At this stage, it is important to separate the issues of flight control and navigation. The navigation algorithms should reside in the navigation block of the GNC module onboard the UAV. The logical architecture is as shown in Figure 3. Its primary function is to generate trajectory parameters such that mission objectives can be met and mission efficiency enhanced. In existing navigation algorithms, ground obstacles

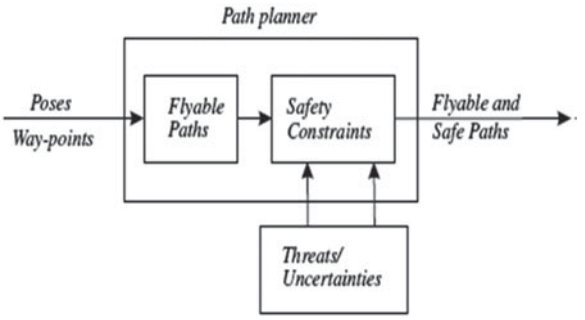

Figure 3. Logical schematic of a navigation block (Shanmugavel et al, 2005).

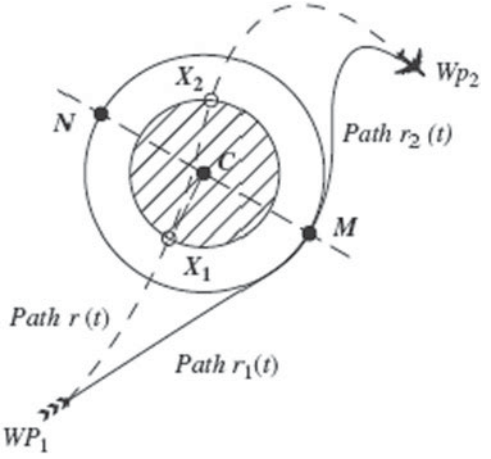

Figure 4. Typical obstacle avoidance trajectory generated by navigational path planner. (Shanmugavel et al, 2005).

are followed or avoided if possible, rather than sought out and exploited. The resulting trajectory in the vicinity of a geophysical feature would resemble the curve depicted in Figure 4. The algorithm proposed in this paper is also a navigation algorithm. Hence, it does not control the motion of the UAV to perform the dynamic soaring loops. On the contrary, it prescribes the technique which allows it to be incorporated into a larger navigation algorithm. What we are trying to propose is to augment the terrain avoidance algorithm with a dynamic soaring algorithm.

In order to harness the advantages of dynamic soaring in a mission, a few things must be known. They are the location of a physical feature, the direction of the wind, the soaring manoeuvres to be performed, the ability to estimate the speed increase, and an algorithm to incorporate the manoeuvres as part of the complete trajectory formation.

Based on previous work, it is recognized that at a flight control level, certain practical devices and set-up modifications are required. Dynamic soaring involves extremely accurate high speed flight in extremely gusty conditions very close to land

https://doi.org/10.1017/S0373463310000378 Published online by Cambridge University Press

features. In order to this, it is assumed that a very robust autopilot capable of controlling rapid dynamics and fitted with proximity sensors is incorporated into the flight control systems.

In the next section, a survey is conducted to determine the dynamic soaring heuristics which are suitable for the scenario concerned. Since the heuristics utilized would determine the start condition of the trajectory in the post-soaring phase, it is important that the most representative be chosen.

2.3. *Dynamic soaring heuristics*. The heuristics of the manoeuvre are as follows. Generally, dynamic soaring manoeuvres are three dimensional, and would involve pitch, yaw and roll. The craft, at constant power, would accelerate with a tailwind. It would also pitch downwards and follow through with a sharply banked turn. The craft would be flying at high speed into a slow speed headwind at the bottom of the slope on the leeward side. It then pitches up. The vertical wind gradient provides additional lift which is translated into an increase in energy. At the top of the wind gradient, it banks hard into the wind, thus completing the loop and having additional speed at the same initial altitude and heading as the start of the loop (see Figure 1).

It is ideally suited to small-scale UAVs due to the nature of the manoeuvre, which involves steep pitches, tightly banked turns and a high rate of acceleration. Models which have been proven to have achieved such flight have been approximately 2–3 metres in wingspan, 1·7 m in length from nose to tail, of conventional configuration, between 1 kg to 1·5 kg weight, and having a reasonably high aspect ratio of around 8, straight trailing edge, no sweepback, half elliptical wing and an airfoil of speed soaring category, such as RG14 or RG15 (see Kinetic 100).

The necessary parameter required to be present in a dynamic soaring heuristic happens to be the velocity function of the UAV. In some earlier studies such as (Zhao and Qi, 2004), in-depth analysis was carried out into the parametric variations of dynamic soaring for both powered and unpowered gliders. It was presumed that the relative ground speed as well as the energy of the UAV remained relatively constant over the period of one cycle. It was also assumed that an energy exchange took place during the flight cycle, between potential energy as a function of altitude over ground level, and kinetic energy, which was a function of flight speed. Actual flight trials of unpowered gliders by dynamic soaring enthusiasts have however consistently proven this assumption to be rather inaccurate. It has been demonstrated that the craft not only increases its actual flight speed over each soaring cycle, but actually increases its flight speed during the climbing stage. However, their paper does not provide the reason why accelerated flight occurs not just during the dive phase of the manoeuvre, but at all stages of the manoeuvre, resulting in a net increase of flight speed in each cycle.

It must also be noted that the heuristics included in the study have to take into consideration the existence of a propulsion unit onboard the UAV to ensure constant speed during straight and level flight. These points were very much focused upon during the literature review for the search of a suitable dynamic soaring heuristic model.

The very first in-depth study done for dynamic soaring was done by (Wharington, 2004). He carried out an in-depth analysis of dynamic soaring heuristics, focusing on harnessing speed and lift by manoeuvring within air layers. He managed to integrate a glide slope function or sink relation, updraft and horizontal wind gradient function,

and bank-pitch commands. Despite this detailed analysis, his paper still maintains that the open loop heuristics can best be described by a sinusoidal airspeed function with a vertical wind gradient. Also unfortunately, his heuristics do not provide a function to predict the speed gain per loop of manoeuvre.

These manoeuvre commands were derived in order to design a closed loop controller which would be able to control a craft to achieve autonomous dynamic soaring. In (Wharington, 2004), the control system resides within the flight control block. No mention is made of the incorporation of his work into the larger realm of mission navigation and trajectory planning.

Lawrence and Sukkarieh in (Lawrence and Sukkarieh, 2009) however address this issue well, and specifically focus upon key parameters which affect the success of dynamic soaring, which are wind gradient, glide slope angle and speed gain. The axial speed, V, variation with real flight time, t, is defined by the following equation:

$$\frac{dV}{dt} = \frac{-\rho S C_{D,0}}{2m} V^2 - \frac{m}{1/2 \rho S \pi e A R} \left[\frac{g \cos\gamma}{V} - \sin^2\gamma \frac{dW_x}{dy} \right]^2 - g \sin\gamma - V \sin\gamma \cos\gamma \frac{dW_x}{dy} \tag{1}$$

The first and second terms describe the complete drag polar, namely form drag and drag due to lift. The third term from the equation is the contribution of flight speed changes by gravity, while the fourth term is the contribution from a vertical wind speed gradient. The key parameters in the equation are the wind gradient and the flight path angle. It is noticed that the first three terms deal with normal flight. Hence they do not contain the term that represents vertical speed gradient. Under such conditions, flight speed will decrease due to a net drag force under straight and level flight or only increase in a descent. With the existence of a wind gradient and a suitable choice of flight path angle, velocity change takes on a net positive velocity.

Selection of flight path angle, γ, follows the empirical relation given by the following equation:

$$\gamma_{optimum} \approx 0 \cdot 230 V + 7 \cdot 43 \frac{dW_x}{dy} + 20 \cdot 1 \tag{2}$$

In this paper, we refer largely to the dynamic model of Lawrence and Sukkarieh with two distinct changes. The first is that we have assumed that the dynamic is of a powered rather than unpowered glider, which has a power conservation system onboard. Hence, the motor is activated only during the tight turns of the flight in order to sustain the speed gained, but is switched off during the climb and dive. Hence, speed drops are less severe during the turns, resulting in a higher net speed increase per cycle.

The second and more important issue is the guidance and navigation algorithm within which these dynamics are embedded. Giving due attention to the tactical requirements of operational UAVs, the guidance law attempts to utilize the additional flight speed to shorten the flight time between two designated waypoints in a route.

A few additional interesting points were noted during the simulation of dynamic soaring utilizing the above equation. Although the speed gain during descent was not

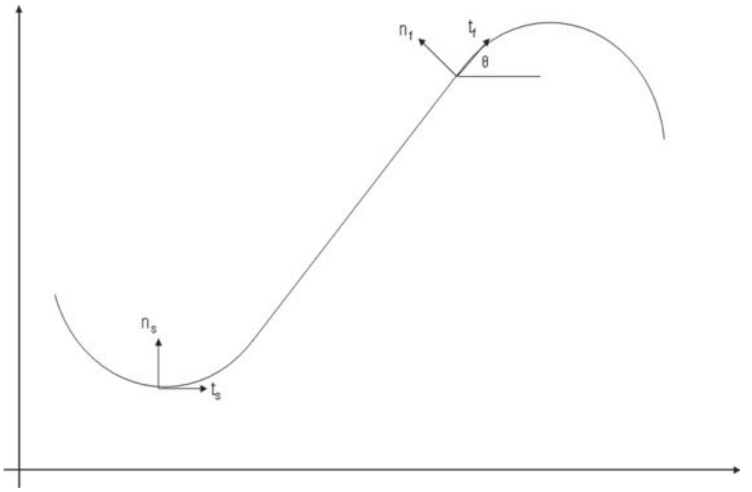

Figure 5. Dubin's curve with a superimposed moving Frenet-Serret frame.

covered in the reference paper, utilizing an angle that was the negative of the climb angle produced the required results. For example, for the glider platform of the specifications used in the paper, the optimal climb angle for a wind speed of 25 ms^{-1} and a wind gradient of 1 ms^{-1}, the optimal climb angle for lift to be generated would be 18·42°. Since dynamic soaring loops, unlike s-shape manoeuvres for gliders which are covered in the paper referenced, are symmetrical with an ascent as well as descent phase, the descent angle was set at $-18{\cdot}42°$.

However, a more significant point was that using the initial speed with optimal climb angle relationship, we found that for a given wind speed gradient, there exists a minimum flight speed below which there is no acceleration but deceleration during the climb. This point, though not explicitly stated in the paper, is a significant factor in guidance and navigation involving dynamic soaring.

3. DIFFERENTIAL GEOMETRY AND DUBIN'S CURVES.

3.1. *Curvature and the moving Frenet Frame.* Differential geometry is a branch of mathematics which utilizes calculus to describe curves and surfaces. Since any trajectory is essentially a mapping of a locus of positions with time, the said trajectory can be represented by a curve. This in turn can be described in a two dimensional plane using only the parameter known as curvature.

A particle which traverses the said trajectory can be considered to be placed at the origin of a moving *Frenet-Serret* frame. The Frenet-Serret frame is a set of three mutually orthogonal vectors, namely, the tangent, normal, and binormal vectors. These vectors, often called **t**, **n**, and **b** vectors, are collectively known as the *Frenet–Serret frame* or *tnb frame*. The frame is defined as follows. Let $s(t)$ represent the arc length which the particle has moved along the curve. The arc length traversed is a function of time. The quantity s is used to give the curve traced out by the trajectory of the particle a natural parameterization by arc length, since many different particle paths may trace out the same geometrical curve by traversing it at

https://doi.org/10.1017/S0373463310000378 Published online by Cambridge University Press

different rates. In detail, s is given by

$$\mathbf{t}' = \mathrm{K}(s)\mathbf{t} = \frac{d\mathbf{t}}{ds} \tag{3}$$

$$\mathbf{n}' = -\mathrm{K}(s)\mathbf{n} = \frac{d\mathbf{n}}{ds} \tag{4}$$

$$\mathrm{K} = \frac{d\theta}{ds} = {}^{1}/_{\rho} \tag{5}$$

Here, $\mathbf{t}$ is the tangent vector, and coincides with the velocity vector, while $\mathbf{n}$ = normal vector, and coincides with the radius of curvature and points towards the instantaneous centre of curvature, K is known as the curvature parameter and ρ is the radius of the curve.

The Frenet-Serret frame, when superimposed onto a moving vehicle, makes certain parameters very clear to visualize and understand (Refer to Figure 5). The instantaneous direction in which the vehicle heads always coincides with the t vector, while n always points towards the centre of the turn circle. If the turn radius is known, the instantaneous position of the centre of the turn circle can be obtained. This vastly reduces computation time for the next step.

3.2. *Dubin's curve and the dynamic soaring path generation.* A Dubin's curve forms the basis of one of the most fundamental ways to join two poses. A pose is a state of a vehicle in time consisting of a position and an attitude (heading if restricted to two dimensions). It would be the joining of a curve (C) with a line (L) with another curve (C) which is (C-L-C).

Since the intended application of the generated navigation algorithm is not for loitering or maintaining a holding pattern but in a point-to-point reconnaissance mission involving a single UAV, the key constraints here would be maximum speed, coupled with shortest distance to complete the mission in the shortest possible time.

Based on the heuristics of dynamic soaring, certain characteristics can be summarized. The speed entering the dynamic soaring loops and the speed exiting would not be the same, as an increase in flight speed is the objective of this manoeuvre. Secondly, due to the high speed of exit, the minimum radius in air without a wind gradient will be far larger. The corresponding conditions at crossover should be input quickly and a trajectory generated within the time constraints.

4. GENERATION OF FLYABLE PATHS.

The calculation for the parameters describing the Dubin's curve is essentially to connect the location and poses between the end of the dynamic soaring manoeuvre and the first waypoint after the geophysical feature. Its key parameters are generated by the navigation block in real time. The navigation block has user-defined waypoints and poses as input.

The two parameters which form the output of the algorithm are firstly the degrees of turn clockwise or anti-clockwise at the start and secondly the degree of turn clockwise or anticlockwise at the end to assume the position and pose at the final waypoint. The maximum g which can be pulled by the uninhabited craft is a fixed, known parameter.

https://doi.org/10.1017/S0373463310000378 Published online by Cambridge University Press

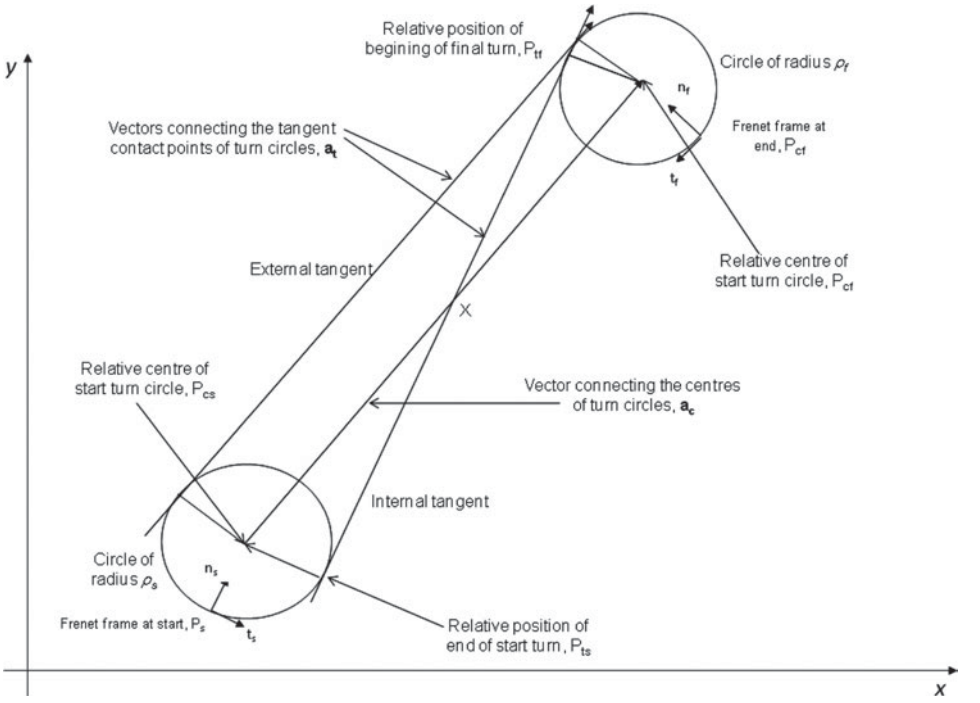

Figure 6. Diagram showing the internal tangent variety of Dubin's curve.

Here, the assumption is made that the high speed developed during the dynamic soaring manoeuvre will be sustained till the next waypoint. Hence, the initial and final turn radii will be identical. Other than this, there are no temporal lower bound conditions which have to be satisfied. We are hence assuming that the trajectory to be generated will have the shortest distance, by virtue of being a Dubin's curve.

At this juncture, the nomenclature to be used in the derivation of the formula is defined. $\vec{\mathbf{a}}$ vectors denote connecting vectors. This means that they connect key points on the initial and final turn circles. $\vec{\mathbf{p}}$ vectors define position vectors, either absolute or relative with respect to the initial and final poses. X and P, however, denote specific geometric points, and have neither magnitude nor direction. The nomenclature used for the subscripts are as follows. We shall use the s subscript for parameters related to the initial turn, and f subscript for parameters related to the final turn. Subscript c is used for any variable denoting the connection of the centres of the two turn circles, while subscript t is used for the tangent connecting the circles mentioned previously. The nomenclature is as illustrated in Figure 6 for both the internal as well as external tangent case.

Working in a Cartesian coordinate system with conventional vector notation (up-right positive and anticlockwise positive for angular measurements), it is assumed that a Frenet frame is superimposed on both the start and end poses. The initial Frenet-Serret frame consists of the unit tangent $\vec{\mathbf{t}}_\mathbf{s}$ and unit normal $\vec{\mathbf{n}}_\mathbf{s}$ vectors, while the final Frenet-Serret frame consists of the unit tangent $\vec{\mathbf{t}}_\mathbf{f}$ and unit normal $\vec{\mathbf{n}}_\mathbf{f}$ vectors. Also, ϑ_s and ϑ_f are the initial heading and final heading changes respectively.

https://doi.org/10.1017/S0373463310000378 Published online by Cambridge University Press

Having defined the known input parameters, we proceed to obtain the position vectors of the centres of the start and final turn circles:

$$\begin{aligned}\vec{\mathbf{p}}_{\mathbf{cs}} &= \vec{\mathbf{p}}_{\mathbf{s}} \pm \rho\vec{\mathbf{n}}_{\mathbf{s}} \\ \vec{\mathbf{p}}_{\mathbf{cf}} &= \vec{\mathbf{p}}_{\mathbf{f}} \pm \rho\vec{\mathbf{n}}_{\mathbf{f}}\end{aligned} \tag{6}$$

The next step would be to obtain the vector joining the centres of the two circles, as follows:

$$\vec{\mathbf{a}}_{\mathbf{c}} = \vec{\mathbf{p}}_{\mathbf{cf}} - \vec{\mathbf{p}}_{\mathbf{cs}} \tag{7}$$

Let P_{cs} and P_{cf} be the points indicating the centres of the initial and final turn circles. Further, $\vec{\mathbf{a}}_{\mathbf{t}}$ is the common tangent vector connecting the two turn circles. By inspection of Figure 6, which is of the internal tangent configuration, we find that there are two triangles. The point where vector $\vec{\mathbf{a}}_{\mathbf{t}}$ and $\vec{\mathbf{a}}_{\mathbf{c}}$ intersect, henceforth called X, is where the vertices of the two triangles meet. Let P_{ts} and P_{tf} be the points of contact of the tangent vector $\vec{\mathbf{a}}_{\mathbf{t}}$ with the initial and final turn circles respectively. Keeping the convention of naming the triangles by their vertices, the triangles with the vertices X P_{ts} Pcs and X P_{tf}Pcf are similar triangles.

Therefore, point X divides the vector $\vec{\mathbf{a}}_{\mathbf{c}}$ according to the ratio of the two radii. This means that:

$$\frac{XP_{cs}}{XP_{cf}} = \frac{P_{ts}P_{cs}}{P_{tf}P_{cf}} = \frac{\rho_s}{\rho_f}. \tag{8}$$

What would be known is the rotation of $\vec{\mathbf{n}}_{\mathbf{s}}$ (i.e. start normal vector) of the initial pose to $\vec{\mathbf{a}}_{\mathbf{c}}$ and $\vec{\mathbf{a}}_{\mathbf{c}}$ to $\vec{\mathbf{n}}_{\mathbf{f}}$ (i.e. final normal vector) of the final pose. The first rotation is referred to as θ_s' and the second as θ_f'. To recap, θ_s and θ_f are the parameters which need to be found.

To obtain θ_s and θ_f, all that needs to be done is to subtract the included angles from each of them, which is $\cos^{-1}\frac{\rho_s}{XP_{cs}}$ or $\cos^{-1}\frac{\rho_f}{XP_{cf}}$. That is:

$$\begin{aligned}\theta_s &= \theta_s' - \cos^{-1}\frac{\rho_s}{XP_{cs}} \\ \theta_f &= \theta_f' - \cos^{-1}\frac{\rho_f}{XP_{cf}}\end{aligned}. \tag{9}$$

Since there is no crossover for the external tangent variety of Dubin's curve, the above formula is modified to become

$$\begin{aligned}\theta_s &= \theta_s' - \frac{\pi}{2} - \sin^{-1}\frac{\rho_s - \rho_f}{|\vec{\mathbf{a}}_{\mathbf{c}}|} \\ \theta_f &= \theta_f' - \cos^{-1}\frac{\rho_s - \rho_f}{|\vec{\mathbf{a}}_{\mathbf{c}}|}\end{aligned} \tag{10}$$

A final check has to be carried out to ensure that necessary and sufficient conditions for the existence of tangents have to be established, and are as follows (refer to Figure 6):

External tangent: $(|\vec{\mathbf{a}}_{\mathbf{c}}| + \rho_s) \geq \rho_f, \rho_s \geq \rho_f$
Internal tangent: $|\vec{\mathbf{a}}_{\mathbf{c}}| > (\rho_s + \rho_f)$

https://doi.org/10.1017/S0373463310000378 Published online by Cambridge University Press

Algorithm used to implement the dynamic soaring technique is as follows:

1. Determine the existence of a set of two waypoints on either side of a known geophysical feature or obstacle.
2. Detect and read the existence of wind above the threshold wind conditions to produce a boundary separation layer in the vicinity of the physical feature.
3. Instead of executing an obstacle avoidance algorithm, begin the implementation of the dynamic soaring algorithm.
4. Execute the closed loop dynamic soaring control algorithm within the stability augmentation module.
5. Based on the speed achieved upon exit, calculate the start and end rotations to traverse the desired Dubin's curve and reach the final position and pose.

The coordinates of the waypoints in step 1 are input by the operator and are stored within the memory of the navigation computer. Surrounding flight data is utilized to obtain the information in step 2. Generally the data from pitot-static or other similar sensors can be used in coordination with data from GPS and Inertial Measurement Units to provide a comprehensive estimate of wind speed and direction. Depending on the parameters of the UAV, a minimum wind speed over the geophysical feature is required to ensure that a speed gain is achieved in both the ascent and descent stages of the dynamic soaring manoeuvre. This point has been discussed in the section on the manoeuvre heuristics. Step 3 involves a decision making algorithm which executes dynamic soaring only if the prevalent wind conditions found in Step 2 are conducive for a substantial speed gain. In step 4, dynamic soaring is executed with the flight path angle as determined by equation 2 and based on wind conditions detected during step 3. It is at this stage that trajectory parameters are computed so as to be executed upon exit of the dynamic soaring stage.

There are two scenarios which we can envisage successfully harnessing the advantages of dynamic soaring. The first is where the waypoint marking the start point of dynamic soaring is on the windward side of the hill and reconnaissance point on the leeward side. The second scenario is where the points are reversed.

There are two reasons why the scenarios where both points are on one side have not been considered. Firstly, there would be no traversing of a geographical feature. Hence, there would not be a terrain avoidance algorithm being executed. Secondly, there would also not be the need for an over-the-hill reconnaissance mission.

5. SIMULATION RESULTS AND DISCUSSIONS. In this section, the trajectory outputs generated by the simulations of the key scenarios in real time are presented. There are two scenarios which have been envisioned. The first is the approach of the land feature from the windward side, and then the approach from the leeward side. The trajectory plots are as shown in Figures 7 and 8 respectively. In each case, the lines have been textured for convenience. The bold oval shape signifies the top of the geological formation. The dotted trajectory shows the path taken by the UAV as it flies from its final waypoint prior to approach and proceeds to transition into the dynamic soaring manoeuvre. The dashed trajectory indicates the

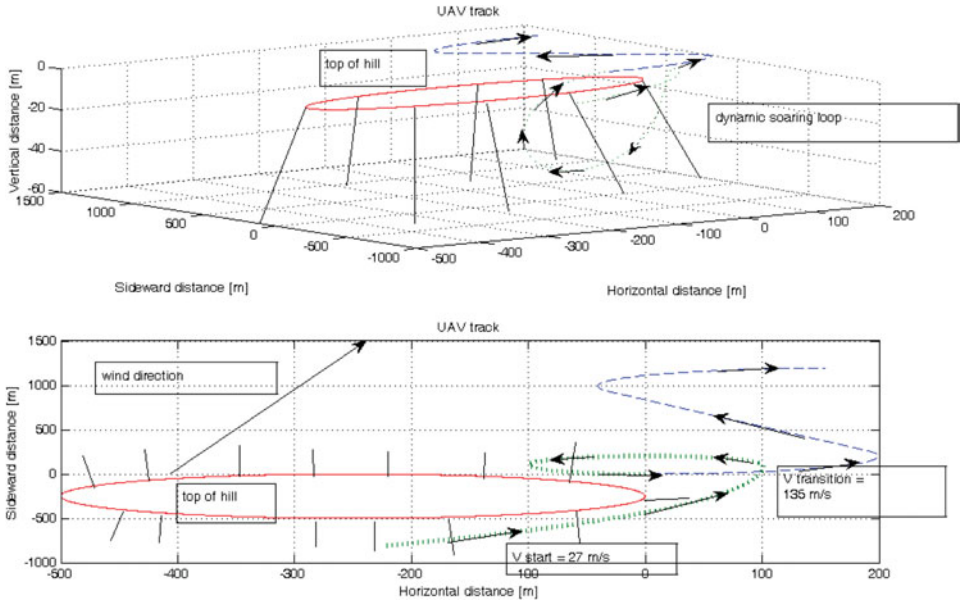

Figure 7. Simulation of trajectory for windwardside approach.

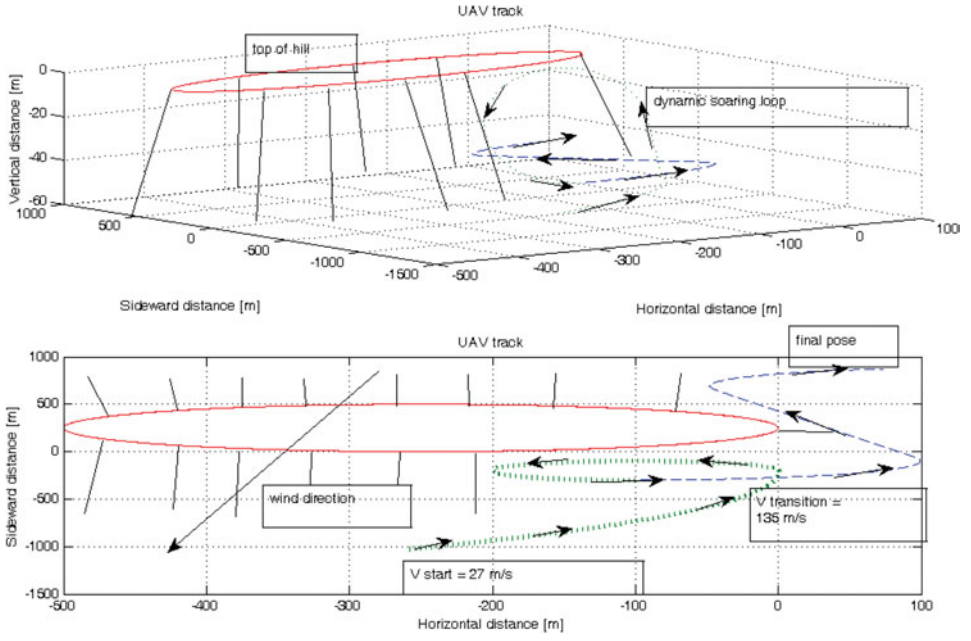

Figure 8. Simulation of trajectory for leeward side approach.

switchover where the UAV exits the dynamic soaring maneuver, having achieved a speed gain, and proceeds to follow a continuous trajectory based on Dubin's curve which had been generated by the algorithm. Kappa values have been given in each

https://doi.org/10.1017/S0373463310000378 Published online by Cambridge University Press

case. They are related to g forces on the UAV based on the formula:

$$n_g = {kv^2}/{gr} \tag{11}$$

5.1. *Windwardside approach.* In this simulation, the final waypoint prior to the dynamic soaring is at coordinates. The hill is of the shape shown in Figure 7. The top of the hill is assumed to be flat. It is signified by a circle of radius 250 m centred at coordinates (−250 m, −250 m) from the centre.

An obstacle avoidance algorithm would generate a trajectory as shown in Figure 4. In this situation, the proposed algorithm generates a trajectory which takes the UAV over the top of the hill, and accelerating with a tail wind. It then follows a glide slope with as specified by equation 2. At the bottom of the slope it executes the sharp bank and climb into the wind characteristic of dynamic soaring manoeuvres. It then repeats the manoeuvre until it has gained sufficient speed, after which it exits to perform the Dubin's curve.

The initial trajectory followed by the dynamic soaring manoeuvre is mapped by the differential geometric parameters: curvature, $K = 1{\cdot}0$; start speed $= 27\ \mathrm{ms}^{-1}$; start altitude $= 0$ m. The outcome of the algorithm proposed in section 4 is as follows for the windward side approach. The turn angle at the start has been 3·78 radians, followed by turn angle at the end of 3·71 radians. Flight speed before soaring is $27\ \mathrm{ms}^{-1}$ (corresponding to approximately 60 miles an hour) and after soaring is $135\ \mathrm{ms}^{-1}$, which corresponds to approximately 300 miles an hour. The middle section consists of a straight path traversed at a speed of $135\ \mathrm{ms}^{-1}$ for 7·01 seconds.

5.2. *Leewardside approach.* In this simulation, the launch point is at coordinates (−250, −1000). The hill is at centred at position (−250 m, 250 m) with a radius of 250 m. The simulation parameters are: curvature, $K = 1{\cdot}0$; speed $= 27\ \mathrm{ms}^{-1}$; start altitude $= -50$ m. In this situation, the dynamic soaring loop begins at the bottom of the hill and loops upwards, thus gaining speed.

The outcome of the algorithm proposed in section 4 is as follows for the leeward side approach. The turn angle at the start has been 3·53 radians, followed by turn angle at the end of 2·71 radians. Flight speed before soaring is $100\ \mathrm{ms}^{-1}$ and after soaring is $135\ \mathrm{ms}^{-1}$. The middle section consists of a straight path traversed at a speed of $135\ \mathrm{ms}^{-1}$ for 7·01 seconds.

The speed gained through the simulation in this case has been approximately 500% over 10 loops of dynamic soaring. As explained in section 2 on dynamic soaring heuristics, the speed gained during each loop depends on the wind gradient developed by the strength of the wind and the flight path angle with respect to the horizontal plane in Earth-centred coordinates. The final speed simply forms the input to the trajectory generation technique. It gives an idea of how fast the trajectory parameters upon exiting the manoeuvre loops must be generated. g value during the final loop was 7·44.

6. CONCLUSIONS AND FUTURE WORK.

This paper aims to demonstrate a viable dynamic soaring algorithm which can be incorporated into the guidance and navigation module of small-scale tactical UAVs. It harnesses the diverse knowledge domains of Dubin's curves and dynamic soaring heuristics to produce a new navigation algorithm.

This brings us to the novelty of the technique proposed in this paper. It harnesses the implicit advantage of the Dubin's curve within the setting of a dynamic soaring trajectory. The advantage lies in its characteristics of simplicity as well as rapid trajectory length and parameter computation. Only data of known terrain contours are required as input for practical implementation. This is the first time Dubin's curve has been used in this context. The key point to this algorithm is its speed and simplicity in arriving at a solution. Given that the g limit of the UAV is known, it is easy to plot a trajectory based on start and end positions and poses given a vastly reduced number of processing steps.

Coupled with the fact that dynamic soaring is all about the maximum possible gain of flight speed, the proposed navigation algorithm promises to further raise the performance standard of small scale tactical UAVs. Through simulation, it has been shown that if implemented successfully, it will greatly enhance the operational effectiveness of the small-scale UAV which is usually deployed in point-to-point, over-the-hill reconnaissance missions. Practically, this means that tactical reconnaissance missions currently carried out by large UAVs which require runways may one day be carried out by much smaller, lighter and cheaper STOL or VTOL UAVs, resulting in improved tactical advantages.

It is recognized that in inclusion of dynamic soaring manoeuvres as part of a trajectory forming algorithm, changes in altitude have to be taken into account. In addition, a slightly different set of temporal constraints have to be considered. This utilizes the heuristics of the dynamic soaring manoeuvres to predict the flight speed gain per revolution of the manoeuvre. This in turn is dependent upon the wind speed detected in the vicinity of the physical feature. The decision to execute dynamic soaring or not is dependent upon the solution of the entire three dimensional trajectory parameters as part of a closed form solution. This is the subject of our subsequent work and publications.

REFERENCES

Akram, M. Imran, Pasha, Ahmed and Iqbal, Nabeel (2005) Optimal Path Planner for Autonomous Vehicles *World Academy of Science, engineering and Technology 3*

Allen, M. J., and Lin, V., (2007) Guidance and control of an autonomous soaring vehicle with flight test results *45th AIAA Aerospace Sciences Meeting and Exhibit 8 - 11 January 2007, Reno, Nevada AIAA 2007-867*

Allen, M. J., (2006) Updraft model for the development of Autonomous soaring Uninhabited Air Vehicles'' *44th AIAA Aerospace Sciences Meeting and Exhibit, 9 - 12 January 2006, Reno, Nevada. AIAA 2006-1510*

Hattenberger, G., Alami, R. and Lacroix, S. (2006) Planning and control for unmanned air vehicle formation flight'' *Proceedings of the 2006 IEEE/RSJ International Conference on Intelligent Robots and Systems October 9 - 15, 2006, Beijing, China*

Langelaan, J. W. and Bramesfeld, G., (2008) Gust energy extraction for mini- and micro-Uninhabited aerial vehicles *46th AIAA Aerospace Sciences Meeting and Exhibit 7 - 10 January, Reno, Nevada AIAA 2008-223*

Langelaan, J. W., (2007) Long distance/duration trajectory optimization for small UAVs *AIAA Guidance Navigation and Control Conference and Exhibit 20 - 23 August Reno, Nevada AIAA 2007-67*

Chitsaz, H. and LaValle, S. M., (2007) Time optimal paths for Dubin's Airplane *46th IEEE Conference on Decision and Control, 12–14 Dec, New Orleans*

Shanmugavel, M., Tsourdos, A., R. Z˙bikowski and B. A. White (2005) Path planning of multiple UAVs using Dubins sets'' *AIAA Guidance, Navigation, and Control Conference and Exhibit 15 - 18 August 2005, San Francisco, California AIAA 2005-5827*

M. Shanmugavel, A. Tsourdos, B. White, R. Z˙bikowski (2009) Co-operative path planning of multiple UAVs using Dubins paths with clothoid arcs "*Control Engineering Practice, in Press 2009.02.010*

J. Kyle, K. Evans, M. Costello (2005) "Atmospheric wind energy extraction by a small autonomous glider" *AIAA Atmospheric Flight Mechanics Conference and Exhibit 15 - 18 August 2005, San Francisco, California AIAA 2005-6233*

Lawrence, Nicholas R. J., and Sukkarieh, Salah (2009) A guidance and control strategy for dynamic soaring with a gliding UAV IEEE International *Conference on Robotics and Automation May 12 - 17 Kobe, Japan*

Yang Guang, and Kapila, Vikram, (2002) Optimal path planning for Unmanned Air Vehicles with Kinematic and Tactical Constraints *Proceedings of the 41st IEEE Conference on Decision and Control, Las Vegas, Nevada WeA04-6*

Yiyuan. J. Zhao and Ying Celia Qi (2004) Minimum fuel powered dynamic soaring of unmanned aerial vehicles utilizing wind gradients *Optimal Control Application and Methods 2004 Volume 25, Issue 5 pp 211-233 Wiley InterScience*

Wharington, John M. (2004) Heuristic control of dynamic soaring *5th Asian Control Conference 2004* Kinetic100 *http://www.dskinetic.com/k100.aspx*